Non-Gaussian behavior in fractional Laplace motion with drift

Wei Wang [1], Yingjie Liang [2,1], Aleksei V. Chechkin [1,3,4,5] and Ralf Metzler [1,5,*]

[1]*Institute of Physics and Astronomy, University of Potsdam, 14476 Potsdam, Germany*

[2]*College of Mechanics and Engineering Science, Hohai University, 211100 Nanjing, China*

[3]*Faculty of Pure and Applied Mathematics, Hugo Steinhaus Center, Wrocław University of Science and Technology, 50-370 Wrocław, Poland*

[4]*German-Ukrainian Core of Excellence, Max Planck Institute of Microstructure Physics, Weinberg 2, 06120 Halle, Germany*

[5]*Asia Pacific Centre for Theoretical Physics, Pohang 37673, Republic of Korea*

(Received 21 November 2024; accepted 21 February 2025; published 18 March 2025)

We study fractional Laplace motion (FLM) obtained from subordination of fractional Brownian motion (FBM) to a gamma process in the presence of an external drift that acts on the composite process or of an internal drift acting solely on the parental process. We derive the statistical properties of this FLM process and find that the external drift does not influence the mean-squared displacement, whereas the internal drift leads to normal diffusion, dominating at long times in the subdiffusive Hurst exponent regime. We also investigate the intricate properties of the probability density function (PDF), demonstrating that it possesses a central Gaussian region whose expansion in time is influenced by FBM's Hurst exponent. Outside of this region, the PDF follows a non-Gaussian pattern. The kurtosis of this FLM process converges toward the Gaussian limit at long times insensitive to the extreme non-Gaussian tails. Additionally, in the presence of the external drift, the PDF remains symmetric and centered at $x = vt$. In contrast, for the internal drift this symmetry is broken. The results of our computer simulations are fully consistent with the theoretical predictions. The FLM model is suitable for describing stochastic processes with a non-Gaussian PDF and long-ranged correlations of the motion.

DOI: 10.1103/PhysRevE.111.034121

I. INTRODUCTION

The stochastic motion of a tracer particle is by-now routinely recorded by single-particle tracking (SPT) experiments in various complex systems [1,2], including biological cells, lipid membranes, polymer solutions, and porous media [3–6]. The observed motion typically deviates from the laws of regular Brownian motion (BM), characterized by the linear time dependence of the mean-squared displacement (MSD) $\langle x^2(t)\rangle \simeq t$ and the Gaussian probability density function (PDF) [7]. Instead, anomalous diffusion is effected, characterized by a power-law form $\langle x^2(t)\rangle \simeq t^\alpha$ of the MSD with the anomalous diffusion exponent α. Subdiffusion with $0 < \alpha < 1$ occurs in systems such as transport in biological cells at the micron- and submicron scales [8–12], for water in the brain of mice or bovine nasal cartilage [13,14], or chemical tracer diffusion in porous media [15–17]. Conversely, superdiffusion with $\alpha > 1$ has been observed, i.a., for diffusion in the interstellar medium on galactic scales [18], animal movement [19,20], endogenous cellular vesicles [21], and solute mixing in groundwater [22,23].

Anomalous diffusion can be effectively captured by various stochastic models tailored to the specific system [25–28]. Among these, the continuous time random walk (CTRW) [24] and fractional Brownian motion (FBM) [29,30] are two prominent processes commonly used to describe anomalous diffusion across a broad range of systems. CTRWs are generalized random walks, in which the motion is defined in terms of a waiting time PDF quantifying trapping events during the motion and a PDF of jump lengths [24,31]. FBM, in turn, is a Gaussian process with stationary, power-law increments, exhibiting antipersistent behavior for the Hurst exponent H in the range $0 < H < 1/2$ and persistent behavior for $1/2 < H < 1$. FBM in the limit $H = 1/2$ corresponds to standard BM. FBM is frequently used to model subdiffusion in viscoelastic environments such as cellular cytoplasm and complex liquids [32–34], as well as superdiffusion in, e.g., amoeboid cells [35]. FBM is also used to model the density profile of nerve fibers in mouse brains [36].

A number of SPT datasets [32,37–40] demonstrate that the statistical properties of the motions originate from multiple underlying mechanisms. Therefore, it is essential to employ mixed processes that exhibit diverse statistical characteristics. Recently, hybrid stochastic processes in the form of generalizations of FBM have been proposed. Examples include FBM combined with CTRW characteristics [41,42], FBM combined with heterogeneous diffusion processes [43,44], and FBM with nonlinear transformations in time or space utilized to describe anomalous diffusion with varying scaling behaviors [45], as well as FBM with stochastic diffusivity [32,46,47]. Additionally, random anomalous exponents were explored in particle ensembles of FBM [48,49].

An alternative extension of FBM can be achieved through subordination. Recent research in geophysics has proposed a

*Contact author: rmetzler@uni-potsdam.de

Published by the American Physical Society under the terms of the Creative Commons Attribution 4.0 International license. Further distribution of this work must maintain attribution to the author(s) and the published article's title, journal citation, and DOI.

model in which hydraulic conductivity is described by subordinating FBM to a gamma process, known as fractional Laplace motion (FLM) [50–53]. Introduced by Meerschaert *et al.* [51], FLM combines FBM as the parent process with a gamma process transforming the operational time of the parent process to a new laboratory time. The gamma process is a strictly increasing Lévy process [54–56] whose increments follow a gamma distribution. The gamma process was first applied by Moran to model water flow into a dam [57], and it is now widely used in different fields, such as maintenance [54], finance [56], or degradation [55]. In the context of subordination theory [58], it represents the trading time or volume in financial applications and the number of depositional features encountered over a distance in hydrology [50]. FLM has been applied successfully in hydraulic conductivity [51,59], subsurface hydrology [60], and sediment transport [52]. Unlike classic FBM or most generalized versions, where the PDFs remain Gaussian or non-Gaussian across all timescales, however, in FLM, the PDFs vary with time: at short times the PDF is non-Gaussian, whereas as the timescale increases, it gradually approaches a Gaussian PDF as quantified by the kurtosis [50].

Here we go one step further and study FLM in the presence of a constant drift. The drift usually arises due to constant force acting on a particle and results in ballistic motion [61–64]. Drift effects are observed in the transient current in an amorphous material with an electric field [65], drying of porous media with temperature and pressure gradients [66], fluctuating interactions in gel electrophoresis [67], or hydrodynamic dispersion in a flow field [68]. In this paper, we consider two distinct drift mechanisms: external drift, which influences the subordinated composite process, and internal drift, which only impacts the parent process. We analyze the statistical properties of the process under two types of drift and explore the complex structure of the PDF as well. We find that over time, a region emerges in which the PDF follows a Gaussian distribution, while outside this region it follows a non-Gaussian distribution. Still, due to the small amplitude of the tail regions, the kurtosis assumes the value of a Gaussian PDF.

This paper is organized as follows. In Sec. II, we recall the characteristic properties of FLM. Sections III and IV are dedicated to deriving the statistical properties of FLM with external and internal drift, respectively—including the moments, MSD, and the kurtosis. We also analyze the intricate structure of the PDFs and the non-Gaussian behaviors. Section V provides the main conclusions.

II. STATISTICAL PROPERTIES OF FLM

FLM $x(t) \equiv B_H(s(t))$ is a process resulting from the subordination of FBM to a gamma process,

$$\frac{dx(s)}{ds} = \zeta_H(s), \quad \frac{ds(t)}{dt} = \varepsilon(s), \tag{1}$$

in the subordination notation in terms of coupled Langevin equations introduced in Refs. [69,70]. Here the parent process $B_H(s)$ is conventional FBM running on the operational time s and driven by the fractional Gaussian noise $\zeta_H(s)$ [30,71] with zero mean and autocovariance function (ACVF),

$$\langle \zeta_H(s_1)\zeta_H(s_2)\rangle \sim 2K_H H(2H-1)|s_1 - s_2|^{2H-2}, \tag{2}$$

where K_H is the generalized diffusion coefficient with physical dimension $[K_H] = \text{length}^2/\text{time}^{2H}$. The PDF of the FBM parent process $B_H(s)$ is Gaussian,

$$G(x,s) = \frac{1}{\sqrt{4\pi K_H s^{2H}}} \exp\left(-\frac{x^2}{4K_H s^{2H}}\right), \tag{3}$$

and the associated MSD is given by

$$\langle x^2(s)\rangle = 2K_H s^{2H}. \tag{4}$$

The subordinator $s(t)$ is the Lévy-Gamma process that is the process with independent stationary increments [72]. The PDF of the subordinator is thus given by

$$h(s,t) = \frac{\lambda^{\gamma t}}{\Gamma(\gamma t)} s^{\gamma t - 1} e^{-\lambda s}, \tag{5}$$

where λ and γ are both parameters of physical dimension time^{-1}. Finally, $\varepsilon(t)$ is the associated gamma noise. Without loss of generality, we use the variable transform $\hat{x} = x/(2K_H\gamma^{2H})^{1/2}$, $\hat{s} = \lambda s$, $\hat{t} = \gamma t$ in Eqs. (1), (3), and (5) to arrive at the corresponding dimensionless forms. In the following, we drop the hat notation for simplicity.

The PDF of the subordinated (or composite) process FLM $x(t) = B_H(s(t))$ is then given in terms of the subordination integral [69,73–76]

$$P(x,t) = \int_0^\infty G(x,s)h(s,t)ds, \tag{6}$$

where $G(x,s)$ and $h(s,t)$ denote the dimensionless PDFs of the parent process $B_H(s)$,

$$G(x,s) = \frac{1}{\sqrt{2\pi s^{2H}}} \exp\left(-\frac{x^2}{2s^{2H}}\right) \tag{7}$$

and of the subordinator $s(t)$:

$$h(s,t) = \frac{1}{\Gamma(t)} s^{t-1} e^{-s}. \tag{8}$$

Using the integral representation of the Fox H-function (Eq. (1.53) in Ref. [77], see also Refs. [78,79]) with parameters $a, b, c > 0$,

$$\int_0^\infty t^{a-1}\exp(-bt - ct^{-\rho})dt = \frac{1}{\rho b^a} H_{0,2}^{2,0}\left[bc^{1/\rho}\middle|\begin{matrix}\\ (a,1),(0,1/\rho)\end{matrix}\right], \tag{9}$$

the PDF (6) of FLM can be expressed via the H-function as

$$P(x,t) = \int_0^\infty \frac{s^{t-H-1}}{\sqrt{2\pi}\Gamma(t)} \exp\left(-\frac{x^2}{2s^{2H}} - s\right)ds = \frac{1}{2H\sqrt{2\pi}\Gamma(t)} \times H_{0,2}^{2,0}\left[\left(\frac{|x|}{\sqrt{2}}\right)^{1/H}\middle|\begin{matrix}\\ (t-H,1),(0,1/(2H))\end{matrix}\right]. \tag{10}$$

In particular, when $H = 1/2$, using the relation between the H-function and the Bessel function (Eq. (1.128) in Ref. [77]), the PDF (10) of FLM becomes

$$P(x,t) = \frac{\sqrt{2/\pi}}{\Gamma(t)}\left(\frac{|x|}{\sqrt{2}}\right)^{t-1/2} K_{t-1/2}(\sqrt{2}|x|), \tag{11}$$

where $K_\alpha(\cdot)$ is the modified Bessel function of the third kind with index α. In the limit $t = 1$, we recover the standard Laplace distribution $P(x, t = 1) = 2^{-1/2}\exp(-\sqrt{2}|x|)$. This key property bestows the process its name, Laplace motion. In the long time limit $t \gg 1$, following the asymptotic behavior of the modified Bessel function for large order μ, given in Appendix A with $z > 0$, we find the approximations

$$K_\mu(z) \sim \begin{cases} \frac{\Gamma(\mu)}{2}\left(\frac{z}{2}\right)^{-\mu}\exp\left(-\frac{z^2}{4\mu}\right), & z \ll \mu \\ \sqrt{\frac{\pi}{2z}}e^{-z}, & z \gg \mu \end{cases}, \tag{12}$$

and the PDF follows a Gaussian form

$$P(x,t) \sim \frac{1}{\sqrt{2\pi t}}\exp\left(-\frac{x^2}{2t}\right) \tag{13}$$

in the regime $|x| \ll t$ and the non-Gaussian form

$$P(x,t) \sim \frac{2^{-t/2}|x|^{t-1}}{\Gamma(t)}\exp(-\sqrt{2}|x|), \tag{14}$$

in the regime $|x| \gg t$.

For arbitrary H, the PDF Eq. (10) of FLM also has a distinct non-Gaussian behavior, namely, for large $|x|$, the PDF (10) asymptotically reads [50]

$$P(x,t) \sim a|x|^{(2t)/(1+2H)-1}\exp(-b|x|^{\frac{2}{1+2H}}), \quad |x| \to \infty, \tag{15}$$

where the factors $a = [\sqrt{1+2H}\Gamma(t)]^{-1}H^{t/(1+2H)-1/2}$ and $b = (1+2H)/2H^{-2H/(1+2H)}$. This non-Gaussian PDF (15) may also be obtained via applying the approximation of the H-function for large $|x|$ as given in Eq. (1.108) in Ref. [77]. In particular, this result is consistent with the special case $H = 1/2$ in Eq. (14).

At long times t, the PDF Eq. (10) can be approximated by the Gaussian PDF:

$$P(x,t) \sim \frac{1}{\sqrt{2\pi t^{2H}}}\exp\left(-\frac{x^2}{2t^{2H}}\right), \quad t \to \infty. \tag{16}$$

The derivation of this asymptotic behavior for the PDF, using the properties of the H-function [80], is provided in Appendix B.

The moments of FLM in subordination form are given by

$$\langle x^n(t)\rangle = \int_0^\infty \langle x^n(s)\rangle h(s,t)ds. \tag{17}$$

Thus, one may immediately obtain the MSD (identical to the second moment) as

$$\langle x^2(t)\rangle = \frac{\Gamma(2H+t)}{\Gamma(t)}. \tag{18}$$

In particular, when $H = 1/2$, FLM displays the linear growth $\langle x^2(t)\rangle = t$ of the MSD at all times. Using the approximation

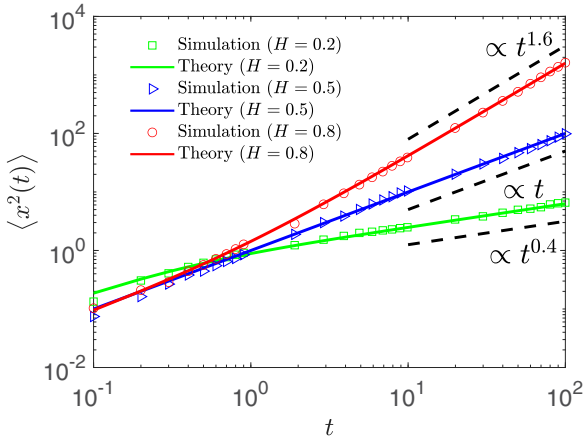

FIG. 1. Simulations (circles, inverted triangles, rectangles) and theoretical results (solid curves) from Eq. (18) of the MSD (1) for FLM for subdiffusive ($H = 0.2$), normal diffusive ($H = 0.5$), and superdiffusive ($H = 0.8$) cases. For details on the simulations of FLM, see Appendix C. Parameters: The trajectory length is $T = 10^2$, the simulation time step of the composite process $x(t)$ is $dt = 0.1$, and that of the operational time s is $ds = dt/10$, the number of trajectories is $N = 300$. These parameters are consistently kept across all figures, unless stated otherwise.

of gamma function (Eq. (6.1.47) in Ref. [81]),

$$z^{b-a}\frac{\Gamma(z+a)}{\Gamma(z+b)} \sim 1 + \frac{(a-b)(a+b-1)}{2z} + o(z^{-1}), \quad z \to \infty, \tag{19}$$

we obtain the MSD of FLM at long times:

$$\langle x^2(t)\rangle \sim t^{2H}. \tag{20}$$

With the fourth-order moment

$$\langle x^4(t)\rangle = 3\frac{\Gamma(4H+t)}{\Gamma(t)}, \tag{21}$$

the kurtosis of FLM κ reads [50]

$$\kappa = \frac{\langle x^4(t)\rangle}{\langle x^2(t)\rangle^2} = 3\frac{\Gamma(4H+t)\Gamma(t)}{\Gamma^2(2H+t)}. \tag{22}$$

At short times, using the approximation $\Gamma(t) \sim 1/t$, the kurtosis has the limiting form

$$\kappa \sim \frac{3\Gamma(4H)}{\Gamma(2H)} \times \frac{1}{t}, \tag{23}$$

implying that in this limit $t \to 0$, the kurtosis assumes an infinite value. At long times, considering terms up to $1/t$ in the leading order expansion of the gamma function in Eq. (19), the approximate kurtosis yields in the form

$$\kappa \sim 3 \times \left(1 + \frac{4H^2}{t}\right). \tag{24}$$

Thus, the kurtosis approaches the Gaussian limit $\kappa = 3$ with as inverse power of time. For $H < 1/2$, the kurtosis decays more rapidly than for $H > 1/2$.

The simulations details to generate FLM are presented in Appendix C. The MSD and the kurtosis of FLM from stochastic simulations for different values of H are shown in Figs. 1 and 2. In both cases, the analytical results are in

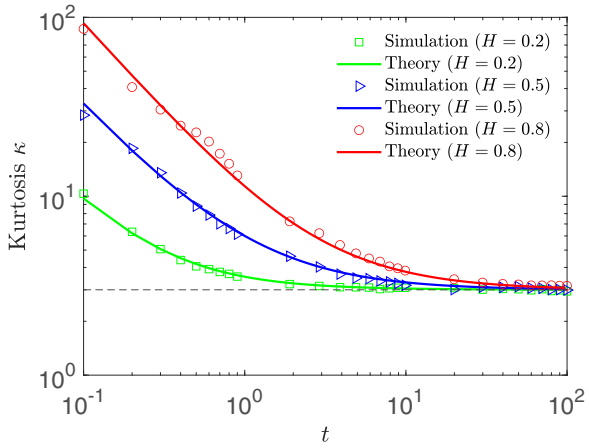

FIG. 2. Kurtosis (1) for FLM. The theoretical result (22) and the long time approximation (24) are in nice agreement with the simulation results. The dashed line represents the Gaussian limit $\kappa = 3$. Parameters: The simulation time step of the operational time s chosen here is $ds = dt/100$, the number of trajectories is $N = 10^4$.

nice agreement with the simulations. The MSD exhibits the power-law scaling t^{2H} at long times. The kurtosis diverges as time approaches zero, and converges to $\kappa = 3$ in the long time limit, indicating the Gaussian nature of the FLM process at long times. Note also the discussion of the peculiar shape of the PDF below.

The increments of the FLM process are given by

$$x_\Delta(t) = x(t+\Delta) - x(t) = B_H(s(t+\Delta)) - B_H(s(t)). \quad (25)$$

On their basis and using the ACVF [50], the mean-squared increment (MSI) of FLM is given by

$$\langle x_\Delta^2(t)\rangle = \frac{\Gamma(2H+\Delta)}{\Gamma(\Delta)}. \quad (26)$$

The MSI is stationary and solely depends on the lag time. Moreover, it is identical to the MSD (18). At large Δ, the MSI reads

$$\langle x_\Delta^2(t)\rangle \sim \Delta^{2H}. \quad (27)$$

The ACVF of the two increments $x(t_1+\Delta) - x(t_1)$ and $x(t_2+\Delta) - x(t_1)$ follows, for any $t_1, t_2 > 0$, in the form

$$\langle x_\Delta(t_1)x_\Delta(t_2)\rangle = \frac{1}{2}\left(\frac{\Gamma(2H+|t_2-t_1+\Delta|)}{\Gamma(|t_2-t_1+\Delta|)} + \frac{\Gamma(2H+|t_1-t_2+\Delta|)}{\Gamma(|t_1-t_2+\Delta|)} - 2\frac{\Gamma(2H+|t_1-t_2|)}{\Gamma(|t_1-t_2|)}\right). \quad (28)$$

Moreover, when $|t_2 - t_1| \gg 1$, the ACVF has the asymptotic power-law form

$$\langle x_\Delta(t_1)x_\Delta(t_2)\rangle \sim H(2H-1)\Delta^2|t_2-t_1|^{2H-2}. \quad (29)$$

This result is similar to the fractional Gaussian noise ACVF (2).

One can also define the fractional Laplace noise:

$$\eta(t) = \frac{x_\Delta(t)}{\Delta}. \quad (30)$$

Then the ACVF of $\eta(t)$ with $|t_2 - t_1| \gg 1$ reads

$$\langle \eta(t_1)\eta(t_2)\rangle \sim H(2H-1)|t_2-t_1|^{2H-2}. \quad (31)$$

When $t_1 = t_2 = t$, the variance of the fractional Laplace noise is

$$\langle \eta^2(t)\rangle = \frac{\Gamma(2H+\Delta)}{\Gamma(\Delta)\Delta^2}. \quad (32)$$

According to the statistical properties of the MSD (20), the MSI (27), the ACVF of the increments (29), and the kurtosis (24), FLM is identical to FBM in the long time limit.

III. EXTERNAL DRIFT ACTING ON THE COMPOSITE FLM PROCESS

To assess the influence of an external drift on the FLM dynamics, we first study the case when the drift acts on the composite FLM process $B_H(s(t))$. The associated Langevin equation is then given by

$$\frac{dx(t)}{dt} = \eta(t) + v, \quad (33)$$

where the drift v is a constant and $\eta(t)$ is the fractional Laplace noise defined in Eq. (30), obeying $\eta(t)dt = [B_H(s(t+dt)) - B_H(s(t))]$.

The simulation approach for generating the FLM with either external or internal drift is presented in Appendix C. Figure 3 illustrates the distinct trajectories of FLM with either external or internal drift (discussed in the next section) $v = 1$. In Fig. 3(a), during a time interval $[t, t+\Delta]$, the gamma process $s(t)$ progresses by the small increment $s_\Delta(t) = s(t+\Delta) - s(t) \ll 1$ (as evidenced by the blowup corresponding to the highlighted dashed rectangle). As seen in Fig. 3(b), FLM with internal drift, acting exclusively on the parent process (52), experiences a small change over the same period as the increment of the process $x(t)$ during the same time window, given by $x_\Delta(t) = B_H(s+s_\Delta) - B_H(s+s_\Delta) = (v+\zeta_H(s)) \times s_\Delta \ll 1$. In contrast, FLM with external drift, Eq. (33), shows a distinct slope, as the drift acts on the composite process. The latter results in an increment $x_\Delta(t) = x(t+\Delta) - x(t) \approx B_H(s(t+\Delta)) - B_H(s(t)) + v\Delta$.

Analogous to the PDF (10) of free FLM, the PDF of FLM with external drift can be obtained as

$$P(x,t) = \int_0^\infty \frac{s^{t-H-1}}{\sqrt{2\pi}\Gamma(t)} \exp\left(-\frac{(x-vt)^2}{2s^{2H}} - s\right)ds = \frac{1}{2H\sqrt{2\pi}\Gamma(t)} \times H_{0,2}^{2,0}\left[\left(\frac{|x-vt|}{\sqrt{2}}\right)^{1/H}\middle|\begin{matrix}\\ (t-H,1),(0,1/(2H))\end{matrix}\right]. \quad (34)$$

When $H = 1/2$, the PDF (34) can be expressed in terms of the modified Bessel function in the form

$$P(x,t) = \frac{\sqrt{2/\pi}}{\Gamma(t)}\left(\frac{|x-vt|}{\sqrt{2}}\right)^{t-1/2} K_{t-1/2}(\sqrt{2}|x-vt|). \quad (35)$$

We note that for all H values, the PDF of FLM with external drift is shifted by vt as compared to the PDF of the free FLM

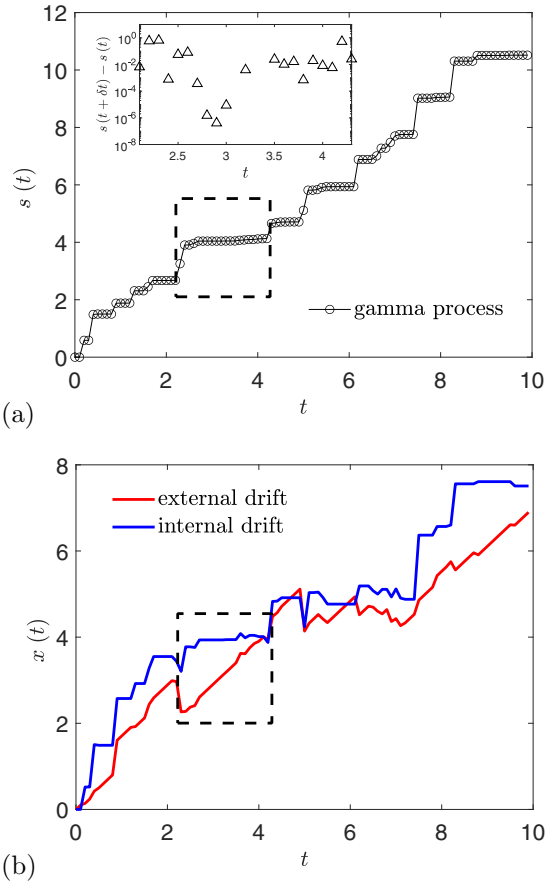

FIG. 3. Trajectories of (a) the subordinator gamma process $s(t)$ and (b) the composite FLM process $x(t)$ of duration $T = 10$ in the presence of an external drift [red curve, Eq. (33)] and an internal drift [blue curve, Eq. (52)]. In (a), each time step of the corresponding trajectory of the gamma process $s(t)$ is represented by circle. During a specific time interval $[t, t + \Delta]$, marked by the dashed rectangle, the gamma process appears to be trapped but is actually displaying variations in its trajectory. The corresponding small but finite increments of $s(t)$ are depicted as the triangles in the inset within the same time interval. During the same time period, also marked by a dashed rectangle in (b), the trajectory of FLM with internal and external drift has distinct behaviors: for internal drift, the trajectory exhibits small increments, while the for the external drift case the motion shows a distinct slope due to the drift. Parameters: $H = 1/2$, $dt = 0.1$.

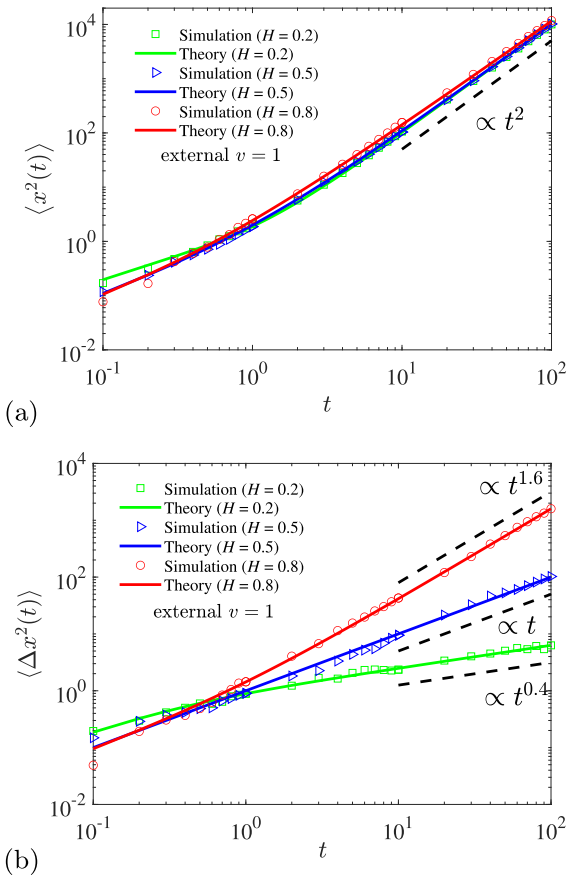

FIG. 4. (a) Second moment and (b) MSD for FLM with external drift $v = 1$. The theoretical results (37) and (38) nicely match the simulations results. The external drift results in ballistic motion in the second moment at long times and has no impact on the MSD.

in Eq. (10). Consequently, the PDF remains symmetric and is centered at $x = vt$.

Due to this Galilei variant behavior, the first moment yields in the form

$$\langle x(t)\rangle = vt. \tag{36}$$

The second moment

$$\langle x^2(t)\rangle = \frac{\Gamma(2H + t)}{\Gamma(t)} + v^2t^2 \tag{37}$$

involves the ballistic shift v^2t^2, and thus the MSD (the second central moment) has the same form as the original FLM process:

$$\langle \Delta x^2(t)\rangle = \frac{\Gamma(2H + t)}{\Gamma(t)}. \tag{38}$$

We note that at long times, the second moment scales as

$$\langle x^2(t)\rangle \sim t^{2H} + v^2t^2, \tag{39}$$

and in this limit the MSD becomes

$$\langle \Delta x^2(t)\rangle \sim t^{2H}. \tag{40}$$

Figure 4 show simulations and theoretical results for the second moment (37) and the MSD (38) for FLM with external drift $v = 1$. The analytical results are in nice agreement with the simulations. At long times, the second moment scales like ballistic motion due to the second term in Eq. (39) which dominates at long times, while the external drift is subtracted out in the MSD (40).

From the Langevin equation (33) with the fractional Laplace noise (30), the ACVF $x_\Delta(t) = x(t + \Delta) - x(t)$ of the increment of FLM with external drift reads

$$\langle x_\Delta(t_1)x_\Delta(t_2)\rangle = \frac{1}{2}\left(\frac{\Gamma(2H + |t_2 - t_1 + \Delta|)}{\Gamma(|t_2 - t_1 + \Delta|)} + \frac{\Gamma(2H + |t_1 - t_2 + \Delta|)}{\Gamma(|t_1 - t_2 + \Delta|)} - 2\frac{\Gamma(2H + |t_1 - t_2|)}{\Gamma(|t_1 - t_2|)}\right) + v^2\Delta^2. \tag{41}$$

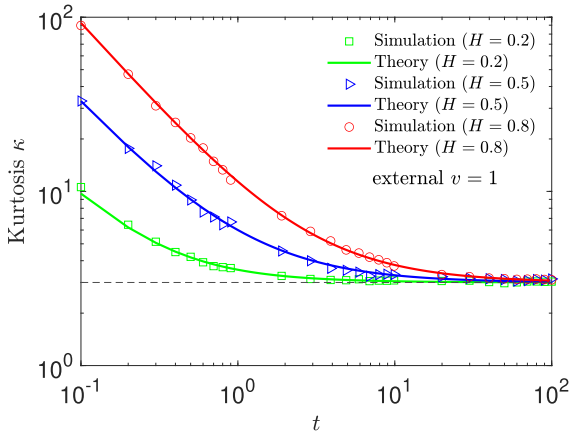

FIG. 5. Kurtosis for FLM with external drift $v = 1$, Eq. (33). The dashed line represents the Gaussian value $\kappa = 3$. As the external has no impact on the kurtosis, the simulation results coincide with the theoretical result (22) for the process without drift. The simulations parameters are the same as those used in Fig. 2.

In particular, when $t_1 = t_2 = t$ (the third term in the parentheses in Eq. (41) vanishes), the MSI yields in the form

$$\left\langle x_\Delta^2(t)\right\rangle = \frac{\Gamma(2H+\Delta)}{\Gamma(\Delta)} + v^2\Delta^2. \tag{42}$$

We note that the MSI (42) is identical to the second moment (37), indicating that the FLM with external drift has stationary increments.

As the external drift has no effect on the central moments, the kurtosis κ of FLM with external drift has the same form as unbiased FLM, as given in Eq. (22). Figure 5 shows simulation results for the kurtosis of FLM with external drift, consistent with the analytical results in Eq. (22).

Using Stirling's formula (Eq. (6.1.37) in Ref. [81]),

$$\Gamma(t) \sim \sqrt{2\pi}t^{t-1/2}e^{-t}, \quad t \gg 1, \tag{43}$$

the PDF (34) can be rewritten as

$$P(x,t) = \frac{1}{2\pi t^{t-1/2}}\int_0^\infty s^{-H-1}\exp(-\phi(s))ds, \tag{44}$$

with the function

$$\phi(s) = \frac{(x-vt)^2}{2s^{2H}} + s - t\ln(s) - t. \tag{45}$$

Based on this approximate formulation we now discuss the asymptotic behaviors of the PDF in the cases $v = 0$ and $v \neq 0$.

A. The unbiased case $v = 0$

When $v = 0$, the function $\phi(s)$ in Eq. (45) becomes $\phi(s) = \frac{x^2}{2s^{2H}} + s - t\ln(s) - t$, attaining a minimum at $s = s_m$. s_m may be obtained by solving $\phi'(s_m) = 0$, producing

$$\frac{t}{s_m} + \frac{Hx^2}{s_m^{2H+1}} = 1. \tag{46}$$

This equation cannot be solved exactly, except for the case $H = 1/2$, when the solution reads $s_m = \frac{1}{2}(t + \sqrt{t^2+2x^2})$. However, it is still possible to obtain an asymptotic solution under specific conditions.

In Eq. (46), it is obvious that $t/s_m < 1$ and $Hx^2/s_m^{2H+1} < 1$. Moreover, if $x^2 \gg t^{2H+1}$, the first term is much less than the second term, and the minimum is attained at $s_m = (Hx^2)^{1/(2H+1)}$. Then the standard Laplace method can be used, and one arrives at the non-Gaussian form (15)

$$\begin{aligned} P(x,t) &\sim \frac{1}{2\pi t^{t-1/2}}s_m^{-H-1}\sqrt{\frac{2\pi}{\phi''(s_m)}}\exp(-\phi(s_m)) \\ &\sim a|x|^{(2t)/(1+2H)-1}\exp(-b|x|^{2/(1+2H)}). \end{aligned} \tag{47}$$

In contrast, when $x^2 \ll t^{2H+1}$, the first term is much larger than the second term in Eq. (46) and the minima is attained at $s_m = t$. Then, the PDF has asymptotic Gaussian form

$$\begin{aligned} P(x,t) &\sim \frac{1}{2\pi t^{t-1/2}}s_m^{-H-1}\sqrt{\frac{2\pi}{\phi''(s_m)}}\exp(-\phi(s_m)) \\ &\sim \frac{1}{\sqrt{2\pi t^{2H}}}\exp\left(-\frac{x^2}{2t^{2H}}\right). \end{aligned} \tag{48}$$

This analysis demonstrates that the PDF $P(x,t)$ is Gaussian inside the interval $(-t^{H+1/2}, t^{H+1/2})$. As time progresses, this interval expands to larger $|x|$ values. However, outside this interval, the PDF is characterized by the non-Gaussian shape (47).

Figure 6 shows the results of our analytical calculations and stochastic simulations of the PDF for FLM without drift at three different times for the Hurst exponents $H = 0.5$, $H = 0.8$, and $H = 0.2$. The analytical results agree well with the simulations in all cases. As predicted, the tails of the PDF are increasingly suppressed by the Gaussian component as function of time, such that the kurtosis becomes decreasingly sensitive to the extreme non-Gaussian tails, as demonstrated in Fig. 2.

B. The biased case $v \neq 0$

When the external drift is nonzero, based on the function $\phi(s)$ from Eq. (45) in the PDF (44) we can obtain a minimum at $s = s_k$, where s_k may be obtained by solving the equation

$$\frac{t}{s_k} + \frac{H(x-vt)^2}{s_k^{2H+1}} = 1. \tag{49}$$

Following the same strategy as used in the case without drift, the solution is $s_k = \frac{1}{2}(t + \sqrt{t^2 + 2(x-vt)^2})$ when $H = 1/2$. When $(x-vt)^2 \gg t^{2H+1}$, the first term is much less than the second term in Eq. (49), and the minimum is attained at $s_k = (H(x-vt)^2)^{1/(2H+1)}$. Then the standard Laplace method can be used again, and one can arrive at the non-Gaussian shape

$$\begin{aligned} P(x,t) &\sim \frac{1}{2\pi t^{t-1/2}}s_k^{-H-1}\sqrt{\frac{2\pi}{\phi''(s_k)}}\exp(-\phi(s_k)) \\ &\sim a|x-vt|^{(2t)/(1+2H)-1} \\ &\quad \times \exp(-b|x-vt|^{2/(1+2H)}). \end{aligned} \tag{50}$$

In contrast, when $(x-vt)^2 \ll t^{2H+1}$, the first term is much larger than the second term in Eq. (49) and the minimum is attained at $s_k = t$. Then, the PDF has the asymptotic Gaussian

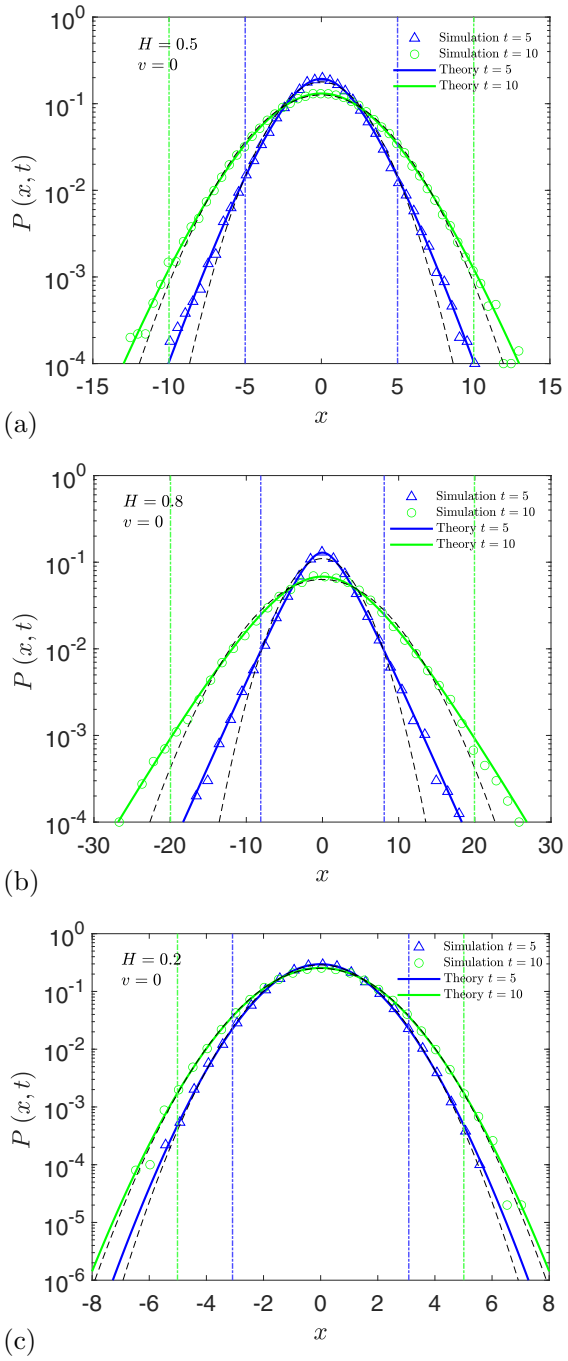

FIG. 6. Simulations (symbols) for the PDF of free FLM at times $t = 5$ and $t = 10$ with (a) $H = 0.5$, (b) $H = 0.8$, and (c) $H = 0.2$. The analytical PDF (colored solid curves) correspond to Eq. (10), while the Gaussian approximation (48) is represented by the dashed curves. The colored vertical lines $x = \pm t^{H+1/2}$ are identified as boundaries separating the Gaussian and non-Gaussian domains.

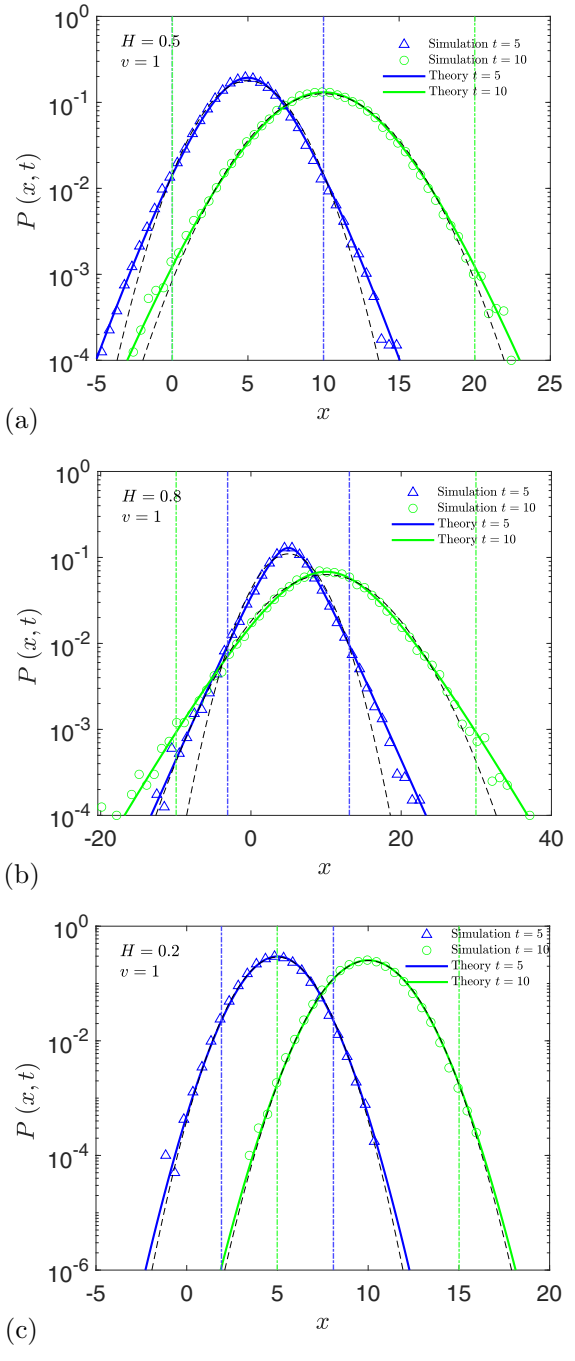

FIG. 7. Simulations (symbols) for the PDF of FLM with external drift $v = 1$, Eq. (33), at $t = 5$ and $t = 10$ with (a) $H = 0.5$, (b) $H = 0.8$, and (c) $H = 0.2$. The analytical results (colored solid curves) are taken from Eq. (34). The Gaussian approximations (dashed curves) correspond to Eq. (51). The colored vertical lines $x = vt \pm t^{H+1/2}$ are identified as boundaries separating the Gaussian and non-Gaussian regimes. In particular, for $H = 0.5$, the left boundaries at all times t are $x = 0$.

form

$$P(x,t) \sim \frac{1}{2\pi t^{t-1/2}} s_k^{-H-1} \sqrt{\frac{2\pi}{\phi''(s_k)}} \exp(-\phi(s_k)) \sim \frac{1}{\sqrt{2\pi t^{2H}}} \exp\left(-\frac{(x-vt)^2}{2t^{2H}}\right). \tag{51}$$

Figure 7 shows the results of our analytical calculations along with results from stochastic simulations of the PDF for FLM with external drift $v = 1$ acting on the subordinated process $x(t)$ for the Hurst exponents $H = 0.5$, $H = 0.8$, and $H = 0.2$. The analytical results agree well with the simula-

tions for all cases. The PDFs are symmetric and centered at $x = vt$. Within the region $(vt - t^{H+1/2}, vt + t^{H+1/2})$, one can clearly identify the Gaussian shape from Eq. (51), while the non-Gaussian behavior (50) is observed outside this region.

IV. INTERNAL DRIFT ACTING SOLELY ON THE PARENT PROCESS

We now consider the FLM $B_H(s(t))$ with internal constant drift v solely acting on the parent process s, i.e.,

$$\frac{dx(s)}{ds} = v + \zeta_H(s), \quad \frac{ds(t)}{dt} = \varepsilon(s). \tag{52}$$

The integral expressions of the PDF of FLM with internal drift is then given by

$$P(x,t) = \int_0^\infty \frac{s^{t-H-1}}{\sqrt{2\pi}\Gamma(t)} \exp\left(-\frac{(x-vs)^2}{2s^{2H}} - s\right) ds. \tag{53}$$

In particular, for $H = 1/2$, the PDF can be expressed in terms of the modified Bessel function:

$$P(x,t) = \frac{\sqrt{2/\pi}}{\Gamma(t)} \left(\frac{|x|}{\sqrt{v^2+2}}\right)^{t-1/2} \times \exp(vx) K_{t-1/2}(\sqrt{v^2+2}|x|). \tag{54}$$

The first moment is again given by the linear growth in time

$$\langle x(t)\rangle = vt, \tag{55}$$

while in the second moment

$$\langle x^2(t)\rangle = \frac{\Gamma(2H+t)}{\Gamma(t)} + v^2 \frac{\Gamma(2+t)}{\Gamma(t)} = \frac{\Gamma(2H+t)}{\Gamma(t)} + v^2(1+t)t, \tag{56}$$

the v-dependent term is given by $v^2(1+t)t$ instead of v^2t^2. Therefore, a term proportional to v^2 remains in the second central moment:

$$\langle \Delta x^2(t)\rangle = \frac{\Gamma(2H+t)}{\Gamma(t)} + v^2 t. \tag{57}$$

Using the approximation of the gamma function (19), we find the long time limit of the second moment

$$\langle x^2(t)\rangle \sim t^{2H} + v^2t^2 \tag{58}$$

and the MSD

$$\langle \Delta x^2(t)\rangle \sim t^{2H} + v^2 t. \tag{59}$$

Figure 8 displays simulations results for the second moment for FLM with internal drift ($v = 1$), Eq. (56), and the associated MSD, Eq. (57), for different values of H. We also show the analytical results, which are in good agreement with the simulations. The behavior of these moments for FLM with internal drift are distinctly different from the case of an external drift shown in Fig. 4. Both types of drifts lead to ballistic motion in the second moment at long times, as indicated by expressions (39) and (57). However, while the external drift does not affect the MSD (40), the internal drift leads to an apparent normal diffusion in the MSD (59), which is the dominant scaling at long times for $H < 1/2$.

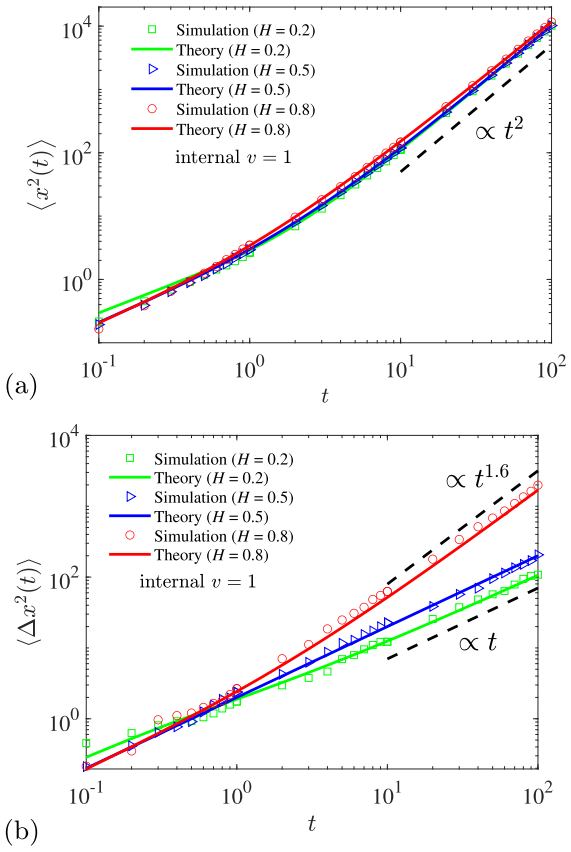

FIG. 8. (a) Second moment and (b) MSD for FLM with internal drift with $v = 1$. The theoretical results from Eqs. (56) and (57) agree nicely with the results from stochastic simulations.

Employing the formula for the ACVF of the displacement of the subordinated process [41,42,82] to FLM with internal drift (52), we obtain

$$\langle x(t_1)x(t_2)\rangle = \tfrac{1}{2}(\langle s^{2H}(t_1)\rangle + \langle s^{2H}(t_2)\rangle - \langle |s(t_2) - s(t_1)|^{2H}\rangle) + v^2\langle s(t_1)s(t_2)\rangle, \tag{60}$$

the ACVF of the increment $x_\Delta(t) = x(t+\Delta) - x(t)$ can be obtained in the form

$$\begin{aligned}\langle x_\Delta(t_1)x_\Delta(t_2)\rangle &= \tfrac{1}{2}(\langle |s(t_1+\Delta) - s(t_2)|^{2H}\rangle + \langle |s(t_1) - s(t_2+\Delta)|^{2H}\rangle \\ &\quad - 2\langle |s(t_1) - s(t_2)|^{2H}\rangle) \\ &\quad + v^2\langle (s(t_1+\Delta) - s(t_1))(s(t_2+\Delta) - s(t_2))\rangle.\end{aligned} \tag{61}$$

For disjoint intervals $[t_1, t_1+\Delta]$ and $[t_2, t_2+\Delta]$, when the increments of the gamma process $s(t)$ are independent, the ACVF (61) becomes

$$\langle x_\Delta(t_1)x_\Delta(t_2)\rangle = \frac{1}{2}\left(\frac{\Gamma(2H+|t_2-t_1+\Delta|)}{\Gamma(|t_2-t_1+\Delta|)} + \frac{\Gamma(2H+|t_1-t_2+\Delta|)}{\Gamma(|t_1-t_2+\Delta|)} - 2\frac{\Gamma(2H+|t_1-t_2|)}{\Gamma(|t_1-t_2|)}\right). \tag{62}$$

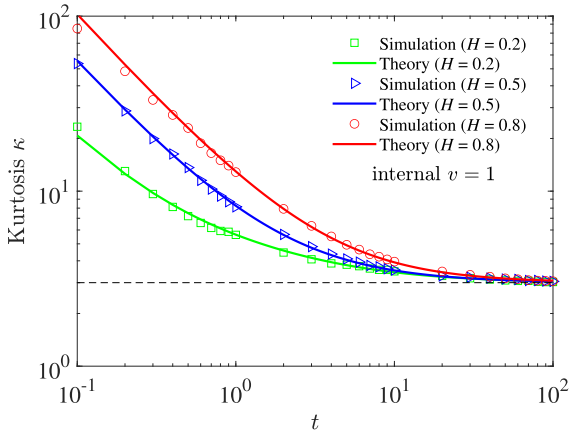

FIG. 9. Simulations and theoretical results, Eq. (64), for the kurtosis for FLM with internal drift ($v = 1$) for varying values of the Hurst exponent H. The dashed line represents $\kappa = 3$.

For $t_1 = t_2 = t$, one can obtain the MSI from Eq. (61),

$$\left\langle x_\Delta^2(t)\right\rangle = \frac{\Gamma(2H+\Delta)}{\Gamma(\Delta)} + v^2(1+\Delta)\Delta, \tag{63}$$

which is stationary and identical to the second moment (56).

The kurtosis κ can be written as the ratio

$$\kappa = \frac{\langle \Delta x^4(t)\rangle}{\langle \Delta x^2(t)\rangle^2} \tag{64}$$

of the central moments, where $\langle \Delta x^4(t)\rangle$ is the fourth central moment given by

$$\langle [x(t) - \langle x(t)\rangle]^4\rangle = 3\left\{\frac{\Gamma(4H+t)}{\Gamma(t)} + v^4(t+2)t + 2v^2\frac{\Gamma(2H+t)}{\Gamma(t)}[t + 2H(2H+1)]\right\}. \tag{65}$$

In the special case $H = 1/2$, the kurtosis assumes the algebraic form

$$\kappa = 3\left(1 + \frac{2}{t} - \frac{1}{(1+v^2)^2 t}\right). \tag{66}$$

The latter approaches the Gaussian value 3 in the long time limit. The latter result is consistent with the expression (22) when $v = 0$.

Figure 9 displays the analytical results and simulations for the kurtosis for FLM with internal drift as a function of time, based on Eq. (64), showing good agreement. Compared to FLM without drift shown in Fig. 2, the kurtosis for FLM with internal drift displays larger values at shorter times and approaches the Gaussian value of $\kappa = 3$ more slowly at long times, as indicated by Eq. (66).

The PDF (53) can be rewritten in the same form we introduced in Eq. (44). Now the function $\phi(s)$ assumes the form

$$\phi(s) = \frac{(x - vs)^2}{2s^{2H}} + s - t\ln(s) - t. \tag{67}$$

In what follows, we discuss the asymptotic behavior of the PDF for the case $v \neq 0$.

When the drift is nonzero, the function (67) assumes a minimum at $s = s_n$, where $\phi'(s_n) = 0$. This leads is to the implicit equation

$$\frac{t}{s_n} + \frac{Hx^2}{s_n^{2H+1}} + \frac{(1-2H)vx}{s_n^{2H}} + \frac{(H-1)v^2}{s_n^{2H-1}} = 1. \tag{68}$$

This relation can be solved exactly when $H = 1/2$, with the solution $s_n = (t + \sqrt{t^2 + (2+v^2)x^2})/(2+v^2)$. In addition, when $x^2 \gg t^2$, $s_n \sim |x|/\sqrt{v^2+2}$. Then the standard Laplace method can be applied, and one can estimate the PDF by the non-Gaussian distribution

$$P(x,t) \sim \frac{1}{2\pi t^{t-1/2}} s_n^{-3/2}\sqrt{\frac{2\pi}{\phi''(s_n)}}\exp(-\phi(s_n)) \sim \overline{a}|x|^{t-1}\exp(-\overline{b}|x|), \tag{69}$$

where we introduced the abbreviations $\overline{a} = (v^2+2)^{-t/2}/\Gamma(t)$ and $\overline{b} = \sqrt{v^2+2} - v\,\mathrm{sgn}(x)$. This non-Gaussian PDF may also be obtained from application of the asymptotic behavior (12) of the modified Bessel in Eq. (54). Unlike the PDF of FLM with external drift, which is symmetric and centered at $x = vt$, see Eq. (50), the non-Gaussian PDF of FLM with internal drift is not symmetric when $v \neq 0$, as shown in Fig. 10(a), and when $v = 0$ it is reduced to Eq. (15).

The Laplace method can also be applied to obtain the approximation of the PDF in the regime $|x| \ll t$, but this PDF cannot help us to capture the behavior of the Gaussian domain of the PDF at long times because the PDF is shifting with vt as indicated by the first moment Eq. (55). However, according to the statistical properties of the process at long times, see above, we can reasonably assume that the central portion of the PDF follows the Gaussian distribution

$$P(x,t) \sim \frac{1}{\sqrt{2\pi(t^{2H} + v^2 t)}}\exp\left(-\frac{(x-vt)^2}{2(t^{2H}+v^2 t)}\right). \tag{70}$$

In Fig. 10, we show stochastic simulations of the PDF for FLM with internal drift ($v = 1$) for the Hurst exponents $H = 0.5$, $H = 0.8$, and $H = 0.2$. Unlike the PDFs with external drift, the PDFs here are no longer symmetry, although they still follow a Gaussian shape, Eq. (70), in certain regions, approximately given by $(vt - t^{H+1/2}, vt + t^{H+1/2})$. For $H = 1/2$, the non-Gaussian behavior of the PDF far from the central part is given by Eq. (69).

V. DISCUSSION AND CONCLUSIONS

We investigate FLM, a generalized diffusion process obtained from subordination of FBM to a gamma process for the drift-free case and in the presence of both an external and an internal drift v. The moments and MSDs of these two types of drift show significantly different behaviors. While in both formulations the second moment is ballistic at long times, the long time scaling of the MSDs are $\simeq t^{2H}$ for external drift and a combination of $\simeq t^{2H}$ and $\simeq t$ for internal drift. The latter thus shows apparently normal diffusion $\simeq t$ at long times when $H < 1/2$. Additionally, we examined the intricate structure of the PDF and identify a central region, whose boundaries expand as function of time, in which the PDF exhibits a Gaussian form. Outside of this region, the

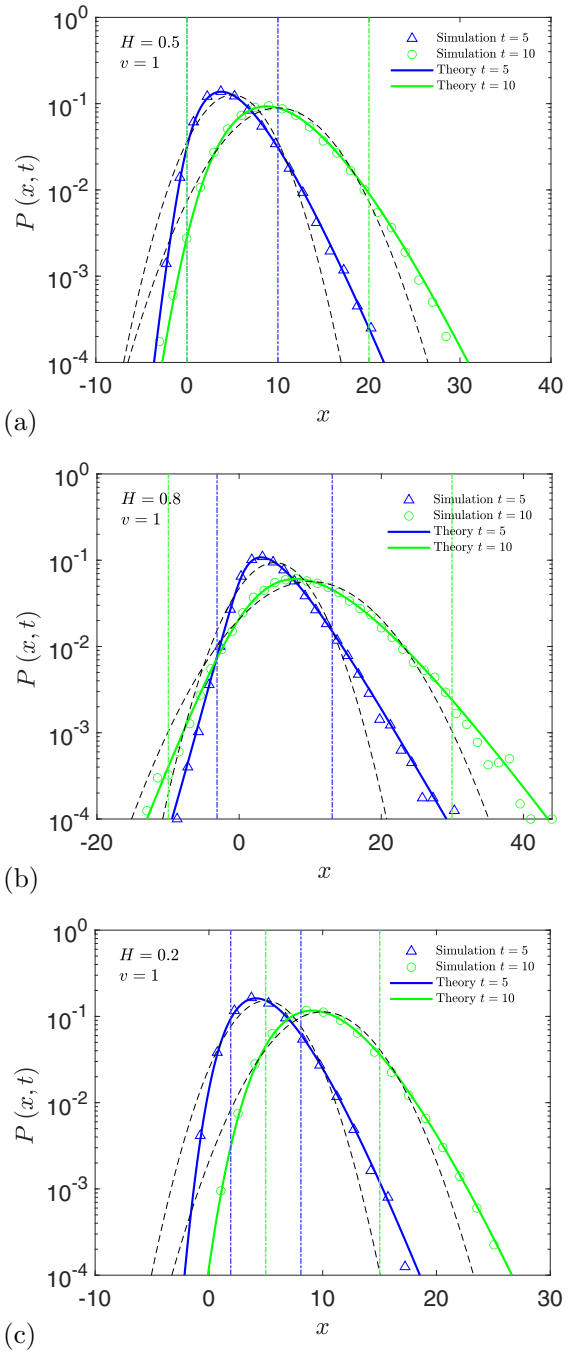

FIG. 10. Simulations (symbols) for the PDF (52) of FLM with internal drift for $v = 1$ and at times $t = 5$ and $t = 10$ with (a) $H = 0.5$, (b) $H = 0.8$, and (c) $H = 0.2$. The analytical results (colored solid curves) correspond to Eq. (53). The Gaussian approximations (dashed curves) are taken from Eq. (70). The boundaries of the Gaussian and non-Gaussian domains $x = vt \pm t^{H+1/2}$ are represented by the colored vertical lines.

PDF remains non-Gaussian. At long times, the non-Gaussian part becomes increasingly suppressed by the central Gaussian region that the kurtosis is no longer sensitive to the non-Gaussian tails. In particular, for an external drift the PDF remains symmetric and centered at $x = vt$, whereas the internal drift breaks this symmetry.

These interesting observations for the PDF can already be observed in the following toy model for the composite, non-Gaussian PDF

$$f(x) = \mathcal{N}[e^{-a/\tau + a^2 - x^2}\theta(a - |x|) + e^{-|x|/\tau}\theta(|x| - a)], \quad (71)$$

in which $\mathcal{N}$ is the normalization constant, $\theta(x)$ is the Heaviside step function, and τ is a scale parameter of the exponential distribution. The PDF (71) has a central Gaussian core for $|x| \leqslant a$ and an exponential tail for $|x| > a$, as shown in Fig. 11. The PDF quickly convergences to a Gaussian with increasing a and its kurtosis approaches the Gaussian value 3. Thus, despite the presence of the non-Gaussian tails, the central Gaussian regime dominates the value of the kurtosis when a increases.

The key distinction between FLM and other comparable stochastic processes such as FBM and Lévy motion lies in the fact that, in the latter two cases, the PDFs of the increments maintain Gaussian and stable distributions across all timescales [27,83,84]. The PDF of FLM rather resembles that of the diffusing diffusivity (DD) model [85–87], recently used to describe Brownian yet non-Gaussian dynamics in various soft matter, biological, and other complex systems [88–95]. The DD model features a characteristic crossover timescale from a non-Gaussian PDF at short times to a Gaussian PDF at long times. Our findings suggest that FLM can serve as an alternative to the DD model for capturing Brownian yet non-Gaussian behavior. However, it is worth noting that the FLM and DD models can be distinguished by analyzing the behavior of the kurtosis κ. In the FLM model, κ approaches infinity in the short-time limit, whereas in the DD model, a value of $\kappa = 9$ (in the one-dimensional version) corresponding to a Laplace distribution with additional power law is observed.

Liang *et al.* [45] recently investigated a subordinated fractional Brownian motion (SFBM) with drift, establishing the PDF via subordination, in a way analogous to Eq. (6). The DD model was also formulated through a subordination approach [86], albeit using a different function $h(s, t)$. The PDF of SFBM remains non-Gaussian throughout the entire time range. Therefore, the transition behavior of the PDF is strongly linked to the statistical properties of the subordination process $s(t)$ or the PDF $h(s, t)$, which should be explored in future studies.

From an experimental perspective, the timescale-dependent non-Gaussian behavior plays a crucial role in FLM-type dynamics. In Refs. [51,59], FLM in the absence of a drift was proposed to examine the increments of hydraulic conductivity data. Standard FLM was extended to accurately capture the sampling timescale-dependent PDF of bed elevation and sediment transport rates in Ref. [52], where the use of operational time was justified by the stochastic nature of turbulent velocity fluctuations near the bed, which introduces randomness in the particle entrainment. With the inclusion of drift, even richer behaviors are expected to emerge in complex systems across hydrology, finance, soft- and biomatter dynamics, as well as turbulence.

ACKNOWLEDGMENTS

Y.L. acknowledges financial support from the Alexander von Humboldt Foundation (Grant No. 1217531), the National

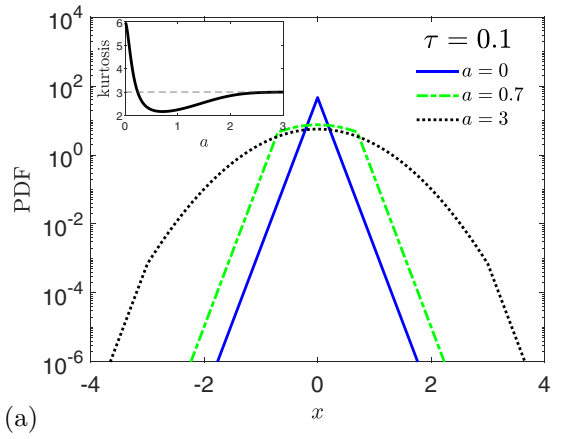

(a)

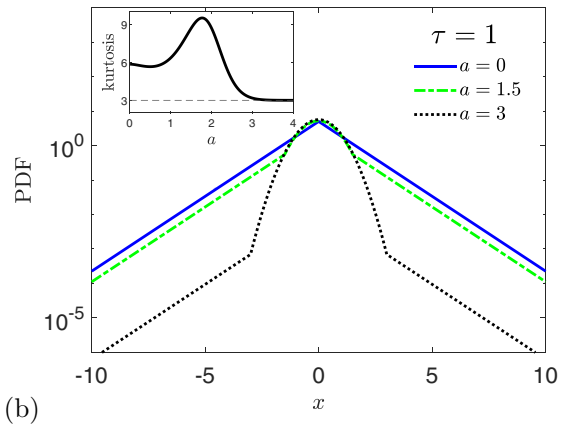

(b)

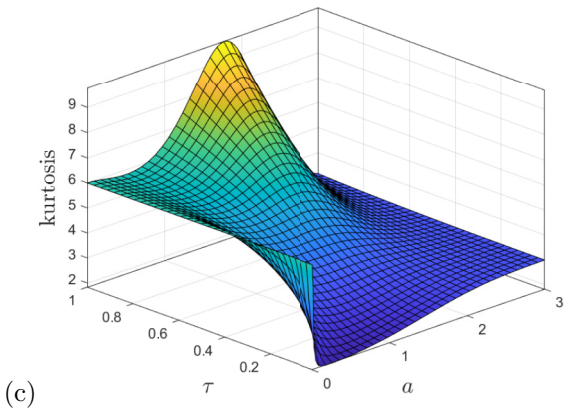

(c)

FIG. 11. PDF (71) with exponential tails for different crossover position a and scale parameters (a) $\tau = 0.1$ and (b) $\tau = 1$. The corresponding kurtosis as a function of a is shown in the inset. (c) The kurtosis as function of a and τ. The behavior of the kurtosis prior to reaching the Gaussian limit value is influenced by the scale parameter τ.

Natural Science Foundation of China (Grant No. 12372382), and the Qing Lan Project of Jiangsu Province (Grant No. 2024). R.M. acknowledges financial support from the German Science Foundation (DFG, Grants No. ME 1535/12-1 and No. ME 1535/16-1) and NSF-BMBF CRCNS (Grant No. 2112862/STAXS). A.V.C. acknowledges BMBF project PLASMA-SPIN Energy (Grant No. 01DK2406).

APPENDIX A: ASYMPTOTIC BEHAVIOR OF $K_\mu(z)$ FOR LARGE ORDER $\mu \gg 1$

The integral representation of the modified Bessel function of the third kind with argument $z > 0$ according to Ref. [81] reads

$$K_\mu(z) = \frac{1}{2}\left(\frac{z}{2}\right)^\mu \int_0^\infty \exp\left(-s - \frac{z^2}{4s}\right)\frac{ds}{s^{\mu+1}}. \tag{A1}$$

The asymptotic expansion of Eq. (A1) can be examined using the Laplace method for large values of the order μ.

First, we rewrite Eq. (A1) in the form

$$K_\mu(z) = \frac{1}{2}\left(\frac{z}{2}\right)^\mu \int_0^\infty \exp\left(-\Phi(s)\right)ds, \tag{A2}$$

with the function

$$\Phi(s) = s + \frac{z^2}{4s} + (\mu+1)\ln(s), \tag{A3}$$

which attains a simple quadratic minimum at

$$s_{\min} = \frac{-(\mu+1) + \sqrt{(\mu+1)^2 + z^2}}{2}. \tag{A4}$$

When $z \gg \mu \gg 1$, we have the quadratic minimum

$$s_{\min} \sim \frac{z}{2} \tag{A5}$$

and use the standard Laplace method. The integral (A1) can be estimated as

$$K_\mu(z) \sim \frac{1}{2}\left(\frac{z}{2}\right)^\mu \sqrt{\frac{2\pi}{|\Phi''(s_{\min})|}}\exp(-\Phi(s_{\min})) \sim \sqrt{\frac{\pi}{2z}}e^{-z}. \tag{A6}$$

We note that this approximation is consistent with the asymptotic behavior of $K_\mu(z)$ for $z \to \infty$ given in Ref. [81].

When $1 \ll z \ll \mu$, the quadratic minimum asymptotically becomes

$$s_{\min} \sim \frac{-\mu + \mu\sqrt{(1 + z^2/\mu^2)}}{2} \sim \frac{z^2}{4\mu}. \tag{A7}$$

Using the Laplace method, we find

$$K_\mu(z) \sim \frac{2^{\mu-1}}{z^\mu}(\sqrt{2\pi}e^{-\mu}\mu^{\mu-1/2})\exp\left(-\frac{z^2}{4\mu}\right) \sim \frac{\Gamma(\mu)}{2}\left(\frac{z}{2}\right)^{-\mu}\exp\left(-\frac{z^2}{4\mu}\right). \tag{A8}$$

This approximation in the regime $z \ll \mu$, to our best knowledge, has not been explored previously. Moreover, although the approximation in Eq. (A8) holds for $1 \ll z \ll \mu$, it is also consistent with $K_\mu(z) \sim [\Gamma(\mu)/2](z/)^{-\mu}$ as $z \to 0$ in Ref. [81].

Figure 12 displays the approximate form of $K_\mu(z)$ for $z \gg \mu$ and $z \ll \mu$, in perfect agreement with the numerical integral (A1).

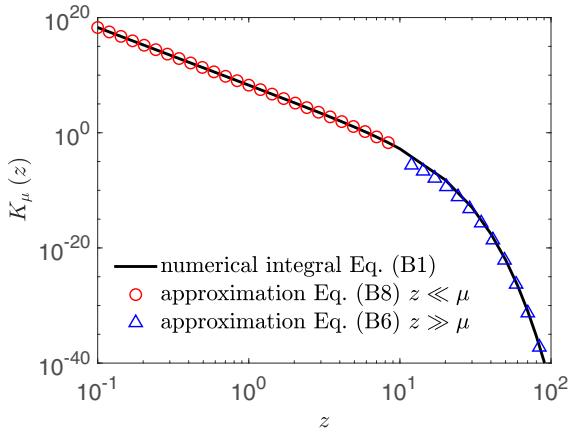

FIG. 12. Modified Bessel function $K_\mu(z)$, Eq. (A1), for large order $\mu = 10$. The blue triangles represent the approximate form (A6) for argument $z \gg \mu$ and the red circles show approximation (A8) for $z \ll \mu$.

APPENDIX B: ASYMPTOTIC BEHAVIOR OF $P(x,t)$ FOR $t \to \infty$ IN EQ. (10)

We rewrite the PDF $P(x,t)$ in Eq. (10) in the form

$$P(x,t) = \frac{1}{2H\sqrt{2\pi}\Gamma(t)}\mathcal{H}\left[\left(\frac{|x|}{\sqrt{2}}\right)^{1/H}\right], \tag{B1}$$

in which the H-function is expressed by the contour integral [77]

$$\mathcal{H}[z] = H^{2,0}_{0,2}\left[z\middle|\begin{matrix}\\ (t-H,1),(0,1/(2H))\end{matrix}\right] \tag{B2}$$

$$= \frac{1}{2\pi i}\int_L \Gamma(t-H+s)\Gamma\left(\frac{s}{2H}\right)z^{-s}ds, \tag{B3}$$

where L is a contour separating the poles of the two gamma functions.

Then, using the property

$$\Gamma(t-H+s) \sim \Gamma(t)t^{-H+s}, \quad t \to \infty \tag{B4}$$

of the gamma function [Eq. (6.1.46) in Ref. [81]], the H-function (B3) can be approximated by

$$\mathcal{H}[z] \sim t^{-H}\Gamma(t) \times \frac{1}{2\pi i}\int_L \Gamma\left(\frac{s}{2H}\right)\left(\frac{z}{t}\right)^{-s}ds. \tag{B5}$$

With the variable transformation

$$\tau = \frac{s}{2H}, \quad y = \left(\frac{z}{t}\right)^{2H}, \tag{B6}$$

we find

$$\mathcal{H}[z] \sim 2Ht^{-H}\Gamma(t)\frac{1}{2\pi i}\int_L \Gamma(\tau)y^{-\tau}d\tau$$

$$\sim Ht^{-H}\Gamma(t)\exp\left(-\left[\frac{z}{t}\right]^{2H}\right). \tag{B7}$$

In Eq. (B7), we applied the inverse Mellin transform [96]

$$\frac{1}{2\pi i}\int_L \Gamma(\tau)y^{-\tau}d\tau = e^{-y}. \tag{B8}$$

Therefore, substituting the H-function (B7) with $z = (|x|/\sqrt{2})^{1/H}$ into the PDF (B1), we arrive at the Gaussian approximation of the PDF when $t \to \infty$, namely,

$$P(x,t) \sim \frac{1}{\sqrt{2\pi t^{2H}}}\exp\left(-\frac{x^2}{2t^{2H}}\right). \tag{B9}$$

APPENDIX C: SIMULATIONS DETAILS

Here we provide the simulation details to generate trajectories of free FLM $x(t) = B_H(s(t))$ at discrete times $t_n = n \times dt$, where $dt = T/N$ is the time step and T the measurement time. To simulate a sample trajectory for FLM $x(t_n)$, we start by generating two separate trajectories: one for the gamma process $s(t_n)$ and another for FBM $B_H(s_k)$. Here the operational time is $s_k = k \times ds$ with the time step ds. Typically, ds is chosen to be much smaller than dt, for instance, $ds = dt/10$. For a given time t_n, we find the corresponding point of the gamma process $s(t_n)$, and there exits a number k, such that $s(t_n)$ falls between adjacent time points s_k and s_{k+1} following

$$k \times ds \leqslant s(t_n) \leqslant (k+1) \times ds. \tag{C1}$$

Subsequently, we assign $x(t_n)$ by forwarding this to FBM at either the preceding or succeeding time point:

$$x(t_n) = B_H(s_k) \quad \text{or} \quad x(t_n) = B_H(s_{k+1}). \tag{C2}$$

The difference between $B_H(s_k)$ and $B_H(s_{k+1})$ becomes negligible when ds is sufficiently small.

The trajectories of FLM (33) with external drift, denoted by $y(t_n)$ here, can be generated by

$$y(t_{n+1}) - y(t_n) = x(t_{n+1}) - x(t_n) + vdt, \tag{C3}$$

where $x(t_n)$ is the free FLM at discrete time t_n generated by (C1) and (C2).

To generate FLM (52) with internal drift, denoted by $z(t_n)$, we incorporate the drift term in step (C2) such that

$$z(t_n) = vs_k + B_H(s_k) \text{ or } \quad z(t_n) = vs_{k+1} + B_H(s_{k+1}). \tag{C4}$$

Finally, we mention that all processes start from the origin $x(0) = y(0) = z(0) = 0$ for simplicity.

[1] H. Shen, L. J. Tauzin, R. Baiyasi, W. Wang, N. Moringo, B. Shuang, and C. F. Landes, Single particle tracking: From theory to biophysical applications, Chem. Rev. **117**, 7331 (2017).

[2] C. Manzo and M. F. Garcia-Parajo, A review of progress in single particle tracking: From methods to biophysical insights, Rep. Prog. Phys. **78**, 124601 (2015).

[3] K. Jaqaman, D. Loerke, M. Mettlen, H. Kuwata, S. Grinstein, S. L. Schmid, and G. Danuser, Robust single-particle tracking in live-cell time-lapse sequences, Nat. Methods **5**, 695 (2008).

[4] J.-H. Jeon, M. Javanainen, H. Martinez-Seara, R. Metzler, and I. Vattulainen, Protein crowding in lipid bilayers gives rise to

non-Gaussian anomalous lateral diffusion of phospholipids and proteins, Phys. Rev. X **6**, 021006 (2016).

[5] J. Shin, A. G. Cherstvy, W. K. Kim, and R. Metzler, Facilitation of polymer looping and giant polymer diffusivity in crowded solutions of active particles, New J. Phys. **17**, 113008 (2015).

[6] M. J. Skaug, L. Wang, Y. Ding, and D. K. Schwartz, Hindered nanoparticle diffusion and void accessibility in a three-dimensional porous medium, ACS Nano **9**, 2148 (2015).

[7] N. G. Van Kampen, *Stochastic Processes in Physics and Chemistry* (Elsevier, 1992).

[8] F. Etoc, E. Balloul, C. Vicario, D. Normanno, D. Lioe, A. Sittner, J. Piehler, M. Dahan and M. Coppey, Non-specific interactions govern cytosolic diffusion of nanosized objects in mammalian cells, Nat. Mater. **17**, 740 (2018).

[9] S. Scott, M. Weiss, C. Selhuber-Unkel, Y. F. Barooji, A. Sabri, J. T. Erler, R. Metzler and L. B. Oddershede, Extracting, quantifying, and comparing dynamical and biomechanical properties of living matter through single particle tracking, Phys. Chem. Chem. Phys. **25**, 1513 (2023).

[10] M. Weiss, M. Elsner, F. Kartberg, and T. Nilsson, Anomalous subdiffusion is a measure for cytoplasmic crowding in living cells, Biophys. J. **87**, 3518 (2004).

[11] I. Golding and E. C. Cox, Physical nature of bacterial cytoplasm, Phys. Rev. Lett. **96**, 098102 (2006).

[12] I. Wong, M. Gardel, D. Reichman, E. Weeks, M. Valentine, A. Bausch, and D. Weitz, Anomalous diffusion probes microstructure dynamics of entangled F-actin networks, Phys. Rev. Lett. **92**, 178101 (2004).

[13] Y. Liang, Q. Y. Allen, W. Chen, R. G. Gatto, L. Colon-Perez, T. H. Mareci, and R. L. Magin, A fractal derivative model for the characterization of anomalous diffusion in magnetic resonance imaging, Commun. Nonlinear Sci. **39**, 529 (2016).

[14] Y. Yu and Y. Liang, Fractal relaxation model with a nonlinear diffusion coefficient for fitting anomalous diffusion data in magnetic resonance imaging, J. Magn. Reson. **355**, 107558 (2023).

[15] S. Yan, Y. Liang, and W. Xu, Characterization of chloride ions diffusion in concrete using fractional Brownian motion run with power law clock, Fractals **30**, 2250177 (2022).

[16] S. Yan and Y. Liang, A space fractal derivative temperature model in characterization of chloride ions superdiffusion in concrete in a marine environment, J. Build. Eng. **78**, 107669 (2023).

[17] A. Rajyaguru, R. Metzler, I. Dror, D. Grolimund, and B. Berkowitz, Diffusion in porous rock is anomalous, Environ. Sci. Technol. **58**, 8946 (2024).

[18] Y. E. Litvinenko, H. Fichtner, and D. Walter, Anomalous transport of cosmic rays in a nonlinear diffusion model, Astrophys. J. **841**, 57 (2017).

[19] N. E. Humphries, N. Queiroz, J. R. M. Dyer, N. G. Pade, M. K. Musyl, K. M. Schaefer, D. W. Fuller, J. M. Brunnschweiler, T. K. Doyle, J. D. R. Houghton *et al.*, Environmental context explains Lévy and Brownian movement patterns of marine predators, Nature (London) **465**, 1066 (2010).

[20] P. G. Meyer, A. G. Cherstvy, H. Seckler, R. Hering, N. Blaum, F. Jeltsch, and R. Metzler, Directedness, correlations, and daily cycles in springbok motion: From data via stochastic models to movement prediction, Phys. Rev. Res. **5**, 043129 (2023).

[21] J. F. Reverey, J.-H. Jeon, H. Bao, M. Leippe, R. Metzler, and C. Selhuber-Unkel, Superdiffusion dominates intracellular particle motion in the supercrowded cytoplasm of pathogenic Acanthamoeba castellanii, Sci. Rep. **5**, 11690 (2017).

[22] Y. Liang, S. Yan, P. Tian, and W. Xu, Characterization of solute mixing in heterogeneous media by means of fractal dilution index, Transp. Porous Med. **148**, 123 (2023).

[23] Y. Liang, Z. Dou, L. Wu, and Z. Zhou, Fast mixing in heterogeneous media characterized by fractional derivative model, Transp. Porous Med. **134**, 387 (2020).

[24] E. W. Montroll and G. H. Weiss, Random walks on lattices. II, J. Math. Phys. **6**, 167 (1965).

[25] A. Mura and G. Pagnini, Characterizations and simulations of a class of stochastic processes to model anomalous diffusion, J. Phys. A: Math. Theor. **41**, 285003 (2008).

[26] J. H. Schulz, E. Barkai, and R. Metzler, Aging renewal theory and application to random walks, Phys. Rev. X **4**, 011028 (2014).

[27] R. Metzler, J.-H. Jeon, A. G. Cherstvy, and E. Barkai, Anomalous diffusion models and their properties: Non-stationarity, non-ergodicity, and ageing at the centenary of single particle tracking, Phys. Chem. Chem. Phys. **16**, 24128 (2014).

[28] W. Wang, R. Metzler, and A. G. Cherstvy, Anomalous diffusion, aging, and nonergodicity of scaled Brownian motion with fractional Gaussian noise: Overview of related experimental observations and models, Phys. Chem. Chem. Phys. **24**, 18482 (2022).

[29] A. N. Kolmogorov, Wienersche Spiralen und einige andere interessante Kurven im Hilbertschen Raum, C. R. (doklady), Acad. Sci. URSS (NS) **26**, 115 (1940).

[30] B. B. Mandelbrot and J. W. van Ness, Fractional Brownian motions, fractional noises and applications, SIAM Rev. **10**, 422 (1968).

[31] H. Scher and E. W. Montroll, Anomalous transit-time dispersion in amorphous solids, Phys. Rev. B **12**, 2455 (1975).

[32] A. Sabri, X. Xu, D. Krapf, and M. Weiss, Elucidating the origin of heterogeneous anomalous diffusion in the cytoplasm of mammalian cells, Phys. Rev. Lett. **125**, 058101 (2020).

[33] J.-H. Jeon, V. Tejedor, S. Burov, E. Barkai, C. Selhuber-Unkel, K. Berg-Sørensen, L. Oddershede, and R. Metzler, In vivo anomalous diffusion and weak ergodicity breaking of lipid granules, Phys. Rev. Lett. **106**, 048103 (2011).

[34] J.-H. Jeon, H. Martinez-Seara Monne, M. Javanainen, and R. Metzler, Anomalous diffusion of phospholipids and cholesterols in a lipid bilayer and its origins, Phys. Rev. Lett. **109**, 188103 (2012).

[35] D. Krapf, N. Lukat, E. Marinari, R. Metzler, G. Oshanin, C. Selhuber-Unkel, A. Squarcini, L. Stadler, M. Weiss, and X. Xu, Spectral content of a single non-Brownian trajectory, Phys. Rev. X **9**, 011019 (2019).

[36] S. Janušonis, N. Detering, R. Metzler, and T. Vojta, Serotonergic axons as fractional Brownian motion paths: Insights into the self-organization of regional densities, Front. Comput. Neurosci. **14**, 56 (2020).

[37] M. Di Pierro, D. A. Potoyan, P. G. Wolynes, and J. N. Onuchic, Anomalous diffusion, spatial coherence, and viscoelasticity from the energy landscape of human chromosomes, Proc. Natl. Acad. Sci. USA **115**, 7753 (2018).

[38] C. Ayaz, L. Tepper, F. N. Brünig, J. Kappler, J. O. Daldrop, and R. R. Netz, Non-Markovian modeling of protein folding, Proc. Natl. Acad. Sci. USA **118**, e2023856118 (2021).

[39] N. A. Bustos, C. M. Saad-Roy, A. G. Cherstvy, and C. E. Wagner, Distributed medium viscosity yields quasi-exponential step-size probability distributions in heterogeneous media, Soft Matter **18**, 8572 (2022).
[40] C. E. Wagner, M. Krupkin, K. B. Smith-Dupont, Ch. M. Wu, N. A. Bustos, J. Witten, and K. Ribbeck, Comparison of physicochemical properties of native mucus and reconstituted mucin gels, Biomacromolecules **24**, 628 (2023).
[41] Z. R. Fox, E. Barkai, and D. Krapf, Aging power spectrum of membrane protein transport and other subordinated random walks, Nat. Commun. **12**, 6162 (2021).
[42] Y. Liang, W. Wang, and R. Metzler, Anomalous diffusion, non-Gaussianity, and nonergodicity for subordinated fractional Brownian motion with a drift, Phys. Rev. E **108**, 024143 (2023).
[43] W. Wang, A. G. Cherstvy, X. Liu, and R. Metzler, Anomalous diffusion and nonergodicity for heterogeneous diffusion processes with fractional Gaussian noise, Phys. Rev. E **102**, 012146 (2020).
[44] W. Wang, A. G. Cherstvy, H. Kantz, R. Metzler, and I. M. Sokolov, Time averaging and emerging nonergodicity upon resetting of fractional Brownian motion and heterogeneous diffusion processes, Phys. Rev. E **104**, 024105 (2021).
[45] Y. Liang, W. Wang, R. Metzler, and A. G. Cherstvy, Anomalous diffusion, nonergodicity, non-Gaussianity, and aging of fractional Brownian motion with nonlinear clocks, Phys. Rev. E **108**, 034113 (2023).
[46] W. Wang, F. Seno, I. M. Sokolov, A. V. Chechkin, and R. Metzler, Unexpected crossovers in correlated random diffusivity processes, New J. Phys. **22**, 083041 (2020).
[47] A. Pacheco-Pozo and D. Krapf, Fractional Brownian motion with fluctuating diffusivities, Phys. Rev. E **110**, 014105 (2024).
[48] D. Han, N. Korabel, R. Chen, M. Johnston, A. Gavrilova, V. J. Allan, S. Fedotov, and T. A. Waigh, Deciphering anomalous heterogeneous intracellular transport with neural networks, eLife **9**, e52224 (2020).
[49] M. Balcerek, K. Burnecki, S. Thapa, A. Wyłomańska, and A. Chechkin, Fractional Brownian motion with random Hurst exponent: Accelerating diffusion and persistence transitions, Chaos **32**, 093114 (2022).
[50] T. J. Kozubowski, M. M. Meerschaert, and K. Podgorski, Fractional Laplace motion, Adv. Appl. Probab. **38**, 451 (2006).
[51] M. M. Meerschaert, T. J. Kozubowski, F. J. Molz, and S. Lu, Fractional Laplace model for hydraulic conductivity, Geophys. Res. Lett. **31**, L08501 (2004).
[52] V. Ganti, A. Singh, P. Passalacqua, and E. Foufoula-Georgiou, Subordinated Brownian motion model for sediment transport, Phys. Rev. E **80**, 011111 (2009).
[53] J. Gajda, A. Wyłomańska, and A. Kumar, Generalized fractional Laplace motion, Stat. Probabil. Lett. **124**, 101 (2017).
[54] J. M. van Noortwijk, A survey of the application of gamma processes in maintenance, Reliab. Eng. Syst. Safe. **94**, 2 (2009).
[55] J. Lawless and M. Crowder, Covariates and random effects in a gamma process model with application to degradation and failure, Lifetime Data Anal. **10**, 213 (2004).
[56] D. B. Madan, P. P. Carr, and E. C. Chang, The variance gamma process and option pricing, Rev. Financ. **2**, 79 (1998).
[57] T. B. Mitchell, A method of estimating the approximate yield of multiple dams using the Moran model, J. Hydrol. **37**, 67 (1978).
[58] S. Bochner, Subordination of non-Gaussian stochastic processes, Proc. Natl. Acad. Sci. USA **48**, 19 (1962).
[59] F. J. Molz, T. J. Kozubowski, K. Podgórski, and J. W. Castle, A generalization of the fractal/facies model, Hydrogeol. J. **15**, 809 (2007).
[60] F. J. Molz and P. D. Hyden, A new type of stochastic fractal for application in subsurface hydrology, Geoderma **134**, 274 (2006).
[61] P. Kubala, M. Cieśla, and B. Dybiec, Diffusion in crowded environments: Trapped by the drift, Phys. Rev. E **104**, 044127 (2021).
[62] M. Krasowska, A. Strzelewicz, G. Dudek, and M. Cieśla, Numerical study of drift influence on diffusion transport through the hybrid membrane, Membranes **12**, 788 (2022).
[63] A. Compte, R. Metzler, and J. Camacho, Biased continuous time random walks between parallel plates, Phys. Rev. E **56**, 1445 (1997).
[64] R. Metzler, J. Klafter, and I. M. Sokolov, Anomalous transport in external fields: Continuous time random walks and fractional diffusion equations extended, Phys. Rev. E **58**, 1621 (1998).
[65] A. I. Rudenko and V. I. Arkhipov, Trap-controlled transient current injection in amorphous materials, J. Non-Cryst. Solids **30**, 163 (1978).
[66] Z. Xiao, D. Yang, Y. Yuan, B. Yang, and X. Liu, Fractal pore network simulation on the drying of porous media, Dry. Technol. **26**, 651 (2008).
[67] E. Yarmola, P. P. Calabrese, A. Chrambach, and G. H. Weiss, Interaction with the matrix: The dominant factor in macromolecular band spreading in gel electrophoresis, J. Phys. Chem. B **101**, 2381 (1997).
[68] S. Redner, J. Koplik, and D. Wilkinson, Hydrodynamic dispersion in a self-similar geometry, J. Phys. A: Math. Gen. **20**, 1543 (1987).
[69] H. C. Fogedby, Langevin equations for continuous time Lévy flights, Phys. Rev. E **50**, 1657 (1994).
[70] S. Eule, V. Zaburdaev, R. Friedrich, and T. Geisel, Langevin description of superdiffusive Lévy processes, Phys. Rev. E **86**, 041134 (2012).
[71] Y. Mishura, *Stochastic Calculus for Fractional Brownian Motion and Related Processes*, Lecture Notes in Mathematics, Vol. 1929 (Springer, Berlin, 2008).
[72] Y. Chen, X. Wang, and W. Deng, Subdiffusion in an external force field, Phys. Rev. E **99**, 042125 (2019).
[73] W. Feller, *An Introduction to Probability Theory and its Applications* (Wiley, New York, 1971).
[74] E. Barkai, Fractional Fokker-Planck equation, solution, and application, Phys. Rev. E **63**, 046118 (2001).
[75] R. Gorenflo and F. Mainardi, Parametric subordination in fractional diffusion processes, in *Fractional Dynamics, Recent Advances*, edited by S. C. Lim, J. Klafter, and R. Metzler (World Scientific, Singapore, 2012), Chap. 10, pp. 229–263.
[76] A. V. Chechkin and I. M. Sokolov, Relation between generalized diffusion equations and subordination schemes, Phys. Rev. E **103**, 032133 (2021).
[77] A. M. Mathai, R. K. Saxena, and H. J. Haubold, *The H-Function: Theory and Applications* (Springer, Berlin, 2009).
[78] A. A. Kilbas and M. Saigo, *H-transforms: Theory and Applications* (CRC Press, Boca Raton, 2004).

[79] A. A. Kilbas and M. Saigo, On the H-function, J. Appl. Math. Stoch. Anal. **12**, 191 (1999).
[80] A. P. Prudnikov and O. I. Marichev, *Integrals and Series: More Special Functions* (Gordon and Breach Science Publishers, New York, 1990).
[81] M. Abramowitz and I. A. Stegun, *Handbook of Mathematical Functions with Formulas, Graphs, and Mathematical Tables* (Dover, New York, 1972).
[82] A. Baule and R. Friedrich, Joint probability distributions for a class of non-Markovian processes, Phys. Rev. E **71**, 026101 (2005).
[83] K. A. Penson and K. Górska, Exact and explicit probability densities for one-sided Lévy stable distributions, Phys. Rev. Lett. **105**, 210604 (2010).
[84] A. Chechkin, V. Gonchar, J. Klafter, R. Metzler, and L. Tanatarova, Stationary states of non-linear oscillators driven by Lévy noise, Chem. Phys. **284**, 233 (2002).
[85] M. V. Chubynsky and G. W. Slater, Diffusing diffusivity: A model for anomalous, yet Brownian, diffusion, Phys. Rev. Lett. **113**, 098302 (2014).
[86] A. V. Chechkin, F. Seno, R. Metzler, and I. M. Sokolov, Brownian yet non-Gaussian diffusion: From superstatistics to subordination of diffusing diffusivities, Phys. Rev. X **7**, 021002 (2017).
[87] R. Jain and K. L. Sebastian, Diffusion in a crowded, rearranging environment, J. Phys. Chem. B **120**, 3988 (2016).
[88] B. Wang, J. Kuo, S. C. Bae, and S. Granick, When Brownian diffusion is not Gaussian, Nat. Mater. **11**, 481 (2012).
[89] B. Wang, S. M. Anthony, S. C. Bae, and S. Granick, Anomalous yet Brownian, Proc. Natl. Acad. Sci. USA **106**, 15160 (2009).
[90] J. M. Miotto, S. Pigolotti, A. V. Chechkin, and S. Roldán-Vargas, Length scales in Brownian yet non-Gaussian dynamics, Phys. Rev. X **11**, 031002 (2021).
[91] F. Rusciano, R. Pastore, and F. Greco, Fickian non-Gaussian diffusion in glass-forming liquids, Phys. Rev. Lett. **128**, 168001 (2022).
[92] A. G. Cherstvy, O. Nagel, C. Beta, and R. Metzler, Non-Gaussianity, population heterogeneity, and transient superdiffusion in the spreading dynamics of amoeboid cells, Phys. Chem. Chem. Phys. **20**, 23034 (2018).
[93] R. Großmann, L. S. Bort, T. Moldenhawer, M. Stange, S. S. Panah, R. Metzler, and C. Beta, Non-Gaussian displacements in active transport on a carpet of motile cells, Phys. Rev. Lett. **132**, 088301 (2024).
[94] D. Wang, R. Hu, M. J. Skaug, and D. K. Schwartz, Temporally anticorrelated motion of nanoparticles at a liquid interface, J. Phys. Chem. Lett. **6**, 54 (2015).
[95] K. C. Leptos, J. S. Guasto, J. P. Gollub, A. I. Pesci, and R. E. Goldstein, Dynamics of enhanced tracer diffusion in suspensions of swimming eukaryotic microorganisms, Phys. Rev. Lett. **103**, 198103 (2009).
[96] F. Oberhettinger, *Tables of Mellin Transforms* (Springer, Berlin, 2012).